Lawrence Berkeley National Laboratory
Lawrence Berkeley National Laboratory

Title
Improved Spatial Resolution in Thick, Fully-Depleted CCDs with Enhanced Red Sensitivity

Permalink
https://escholarship.org/uc/item/9987753b

Author
Fairfield, Jessamyn A.

Publication Date
2005-11-10

eScholarship.org Powered by the California Digital Library
University of California

Improved Spatial Resolution in Thick, Fully-Depleted CCDs with Enhanced Red Sensitivity

Jessamyn A. Fairfield*

Abstract– **The point spread function (PSF) is an important measure of spatial resolution in CCDs for point-like objects, since it can affect use in imaging and spectroscopic applications. We present new data and theoretical developments in the study of lateral charge diffusion in thick, fully-depleted charge-coupled devices (CCDs) developed at Lawrence Berkeley National Laboratory (LBNL). Because they are fully depleted, the LBNL devices have no field-free region, and diffusion can be controlled through the application of an external bias voltage. We give results for a 3512x3512 format, 10.5 µm pixel back-illuminated p-channel CCD developed for the SuperNova/ Acceleration Probe (SNAP), a proposed satellite-based experiment designed to study dark energy. The PSF was measured at substrate bias voltages between 3 V and 115 V. At a bias voltage of 115V, we measure an rms diffusion of 3.7 ± 0.2 µm. Lateral charge diffusion in LBNL CCDs is thus expected to meet the SNAP requirements.**

I. Introduction

Lateral charge diffusion in charge-coupled devices (CCDs) is the drifting of charge carriers in the plane of the CCD as the charges travel from the point of charge carrier generation to the potential wells where the charge is collected. Along with pixel size, lateral charge diffusion is the primary factor determining the spatial resolution of a CCD. In traditional thin CCDs developed for astronomical imaging, the lateral diffusion is approximately equal to the thickness of the field-free region, typically on the order of 10 µm. By contrast, the thick, fully-depleted CCDs developed at Lawrence Berkley National Laboratory (LBNL) [1] have no field-free region; instead, charge created near the backside must drift across the 200-300 micrometers (µm) thick substrate to reach the pixel, roughly ten times further than charge transport in traditional thin CCDs. The thick substrate enhances the detection efficiency and minimizes fringing for near-infrared light; however, lateral charge diffusion increases linearly with substrate thickness. The optimal detector thickness will therefore represent a tradeoff between quantum efficiency and PSF, and will depend on the specific application.

The LBNL devices are fabricated from high-resistivity (10 kΩ/cm), weakly doped, n-type silicon substrate, with p-type channels made from boron implants. They can be fully depleted through the application of a substrate bias voltage, typically in the range of 15–30V for a 200 µm thick CCD. Over-depletion of the substrate through the application of higher bias voltages will act to reduce the charge diffusion by increasing the charge transport velocity. The charge carriers collected by the p-channels in these devices are holes, rather than electrons; this design was chosen for better dark current performance and increased radiation hardness. Recent design changes have resulted in devices that can operate at substrate voltages of at least 200 V.

The LBNL CCDs are well-suited for space and ground-based astronomical imaging and spectroscopy. The devices tested here have been developed specifically for a large pixel-count focal plane for the proposed Supernova/Acceleration Probe [3], a satellite experiment designed to collect ~2000 high-redshift supernovae and carry out a weak-lensing survey to study dark energy. For good quantum efficiency in the near-infrared, the SNAP CCDs will have a substrate thickness of 200 µm, while for optimal resolution for weak lensing, the rms PSF should not be much greater than 4 µm. We describe here the characterization of the lateral charge diffusion in these thick, high voltage CCDs as a function of the applied bias voltage. We use a previously developed technique [2] to measure the point spread function and present results for the latest generation of LBNL CCDs developed for SNAP.

II. Measurement Principle

The virtual knife edge method, originally developed in [2], is based on the Foucault knife edge technique, a commonly used tool for determining the profile of a beam. In a Foucault knife edge experiment, an obstructing device such as a razor blade is placed between the pinhole projector and a detector. The projected beam from the pinhole is scanned across the knife edge. At each scanning step, the beam is incrementally blocked by the knife edge. The light intensity at the detector is measured at each step. Scanning the projected beam across the knife edge several times and assuming a Gaussian beam profile, one can then fit an error function to the data points and calculate the beam width.

The idea behind a virtual knife-edge experiment is similar, but instead of a real obstruction blocking the light, an arbitrary region of the image is defined, called the integration square, over which the signal from the spot is summed. The scan is set up so that the spot moves out of the integration square and changes the integrated intensity values in that square over the course of the scan. The edge of the square has the same function as the edge of the razor blade in a standard knife-edge experiment, hence this technique is called the virtual knife edge. See Fig. 1 for a conceptual illustration. If the total light

Manuscript received November 11, 2005. This work was supported by U.S. Department of Energy contract No. DE-AC03-76SF0098.

J. A. Fairfield is with the Lawrence Berkeley National Laboratory, Berkeley, CA 94720 USA (telephone: 510-486-6378, e-mail: JAFairfield@lbl.gov).

in the integration square is plotted for each step of the scan, the resulting plot resembles an error function with a total rms width given by the convolution of the beam width and the lateral diffusion in the CCD. We subtract off the beam width in quadrature. In practice, the beam width is much smaller than the diffusion and makes a negligible contribution. Fitting an error function to the scan data or a Gaussian to the derivative of the scan data yields two estimates of the lateral charge diffusion. The Gaussian method is preferable, because it is less sensitive to fluctuations at the beginning and end of the scan. We examined both fits as a robustness check. Fig. 2 shows the scan data, fit to an error function, and its derivative, fit to a Gaussian, for a typical data set.

The virtual knife-edge technique sidesteps two problems that have been encountered in previous diffusion measurements: it is independent of the physical pixel size, and there is no scattering from a physical knife edge. To optimize the signal-to-noise ratio, we must adjust the exposure time to have as many photons as possible without saturating the pixels.

III. Experimental Apparatus

The CCD was mounted inside a liquid-nitrogen cooled dewar, pumped down to 10^{-5} torr, and cooled to 133 K. We use a Lakeshore Autotuning temperature controller to control the temperature to within 0.1 K. The dewar is mounted to an aluminum mount, which sits atop a Newport optical table. The front of the dewar has an anti-reflection coated glass window and a shutter. The dewar front is attached to a large wooden box, painted black inside and light-tight. The motorized stage sits inside the box, and the optical fiber bringing the light, as well as signals for the motors and encoders, is passed through a small aluminum bulkhead. The motor stage is capable of *x-y-z* translation, and is carefully aligned with the plane of the CCD so that the *x*-axis is equivalent to the CCD row direction, and the *z*-axis is equivalent to a column. The microstepping motor drivers sit outside the black box and are computer-controlled. See Fig. 3 for a photograph of the apparatus.

The CCD is controlled and read out by a modified Astronomical Research Cameras Gen II controller. It has several boards which read out the CCD. The utility board controls the exposure timing, shutter operation, encoder readout, and *x-y* motion of the projector. The timing board generates digital timing signals to control other circuit boards and communicates with the host computer, and a clock driver board provides analog voltage levels from +10V to -10V for the various clock signals needed. The video board processes and digitizes the video output from the CCD, and supplies digitally programmable DC bias voltages to the CCD. Java-based software manages the controller for data acquisition, and the data are analyzed using IDL tools.

To create a small-diameter, high-intensity light source, we use beam optics that filter and focus light from a Xenon arc lamp. An Oriel monochromator is used to provide 550 nm light, which passes through an optical fiber into the light-tight black box. Inside the black box, the fiber is fed into a brass tube on the *x-y-z* translation stage. The light illuminates a 10 μm pinhole, which is collimated by a 25 mm long brass tube. Scattered light is reduced by a baffle thread on the inside of the brass tube and absorbed by the blackened inner tube surface. The collimated pinhole is then focused on the CCD by a Mitutoyo long working-distance microscope objective, with a working distance of 34 um. The theoretically achievable diameter of the focused light beam was 1 μm.

IV. Experimental Procedure

A. Preliminary Measurements

We measured the beam width with a Foucault knife-edge technique, as described earlier, by installing a razor blade in the beam. We measured a beam size of 1.3 ± 0.1 μm, which is consistent with the theoretical prediction based on the diffraction and geometry of the setup. To focus the spot on the CCD, we start with a substrate voltage of 55V, which over-depletes the substrate. We first center the spot on one pixel; then we adjust the distance from the projector to the CCD using the focus stage, first in increments of 1 mm and then in increments of 0.01 mm, and compare the signal in the nearest neighbor pixels to the central pixel. When the ratio of the two is minimized, the spot is focused. We were able to obtain a focus precision of 20 μm, and could maintain focus for up to eight hours before drift made refocusing necessary.

We used the ratio of opposite neighbors to the central pixel to test whether the focused spot remained on-axis after significant lateral translation, by scanning multiple times in all directions and noting the drift. We found an average drift in the *x*-direction of 0.40 μm per 100 μm of motion in the *z*-direction, and 0.76 μm of drift along the *z*-axis per 100 μm of motion along the *x*-axis. In a normal scan, covering 200 μm along the *x*-axis, the drift was less than 0.5 %, which is not a significant amount of drift.

Pixel-to-pixel non-uniformity can be a complicating issue in lateral diffusion measurements. Because of variations in the fabrication process, different pixels may have slightly different light response. This can be seen in a flat field image, where the CCD is exposed to uniform illumination generated by a light source, an integrating sphere, and a monochromator.

To determine the degree to which this would affect our data, we scanned the spot across several pixels and then plotted the pixel response. We found that the pixel response was uniform to within 2%, well within the error of our diffusion calculation.

B. Diffusion Measurement

Our scans varied in substrate voltage from 3 to 115 V and each had 150 images on average. The scans covered from 10–60 pixels, with intermediate steps from 0.4–40 μm. We had to vary the step size by voltage because lower substrate voltages result in more diffusion and a greater PSF, and thus larger steps were needed to get a good statistical fit. The integration region was also varied with substrate voltage, to ensure that the spot was completely contained within the integration

region. A square of about five times the rms diffusion on each side was used; larger integrating squares would introduce additional read noise and degrade the error on the fit. Fig. 4 shows the spot images at several voltages, demonstrating the variation with voltage.

At low voltages, longer exposure times were necessary, because the large diffusion at these voltages caused charge carriers to drift into neighboring pixels, thus lowering the signal in the center pixel. At high voltages, we had the opposite problem, and were careful to keep the exposure time low enough that the potential wells did not fill, which would saturate the pixels and cause charge leakage from the center pixel to neighboring pixels. The exposure times varied from 0.1 to 10 seconds.

During data taking we monitored the baseline level of the CCD, sometimes called the pedestal, and re-took any data exhibiting abnormal fluctuations due to excess background noise. We also made sure to scan over the same pixels each time, to avoid any potential pixel-to-pixel variation. All of the data were taken with 550 nm light, and all the scans were taken across the channel stops. Previous work has shown that there was no difference between scans in the row and column direction [2].

V. Results

Once the setup was completed and the spot size was characterized, we took data with a device similar to the one previously characterized [2]. We found that the setup gave reliable data and reproduced the previous results, so we installed the new high voltage CCD.

High-voltage testing proceeded with a SNAP large format (3512x3512 pixels), 10.5 µm pixel, 200 µm thick substrate, back-illuminated, boron-doped, p-channel, high-voltage CCD. The rms diffusion measured with a Gaussian fit to the data as a function of substrate voltage is given in Table 1.

A. Theoretical Predictions

Previous theoretical studies of charge diffusion [4] concluded that when the CCD is overdepleted, the diffusion can be quantified by integrating the path of the charge as it travels across the substrate. This formulation, an asymptotic limit of a more complex model that takes field-free regions into account, gives

$$\sigma_{asymp}^2 = 2\frac{k_B T}{q}\frac{z_J^2}{V_{sub} - V_{J'}} \quad (1)$$

as the diffusion, where z_J is the device thickness, V_{sub} is the substrate voltage, $V_{J'}$ is the effective voltage at the p-n junction, T is the temperature, k_B is the Boltzmann constant, and q is the electron (or hole) charge. At low voltages, this equation would still describe the diffusion in the depleted region, but there is now an undepleted region in which the charge is not subject to any electric field. At low voltages, the diffusion is equal to the thickness of the undepleted region. This can be expressed as

$$\sigma_{undepl} = z_J - \sqrt{\frac{2\varepsilon_{Si}}{qN_D}(V_{sub} - V_{J'})}\,, \quad (2)$$

i.e., the thickness of the undepleted region is the thickness of the device minus the thickness of the depleted region [2]. Here, ε_{Si} is the permittivity of silicon, and N_D is the density of dopant atoms. In the voltage regime near the depletion voltage, a convolution of these two expressions describes the diffusion.

In order to compare our data to theory, we first used equation (2) to fit the quantity $(z_J - \sigma_{undepl})^2$, which is linear at low voltages. We extracted the effective junction voltage, the depletion voltage, and the dopant density from this fit, and found a junction voltage of –18.8 V, a depletion voltage of 18.1 V, and a dopant density of $1.2*10^{12}$ carriers per cm^3. Such a fit is shown in Fig. 5. From these parameters we extrapolated the high-voltage asymptotic diffusion given by equation (1).

At voltages well above the depletion voltage, our data were consistently 30-40% higher than theoretical predictions. After repeated checks of the apparatus, beam size, and fit calculations, we remained convinced of the accuracy of our data.

We believe the discrepancy lies in drift velocity saturation of charge carriers. Velocity saturation is expressed as a correction to the carrier mobility [5]. The resulting expression for lateral charge diffusion is

$$\sigma_{asymp}^2 = 2\frac{k_B T}{q}\frac{z_J^2}{m(E,T)(V_{sub} - V_J)}\,, \quad (3)$$

where $m(E,T)$ is the correction factor given by

$$m(E,T) \approx \left[1 + \left(\frac{E}{E_c}\right)^{\beta}\right]^{-1/\beta}. \quad (4)$$

For holes, $E_c = 1.24T^{1.68}$ and $\beta = 0.46T^{0.17}$. E_c is the saturation field at which the drift velocity, υ_d, becomes constant. This correction significantly improves the high-voltage fit, although data points near the substrate voltage are still somewhat off. Investigation of this effect is still underway.

The revised theoretical predictions are plotted versus the data in Fig. 6. The errors plotted with the data are tabulated in Table 1 and are derived from the statistical errors on the measurement.

B. Systematic and Statistical Errors

Once we had taken scans, we checked the robustness of the data in several ways. We examined both the error function and Gaussian fit to verify that the results were comparable. We also examined the data for several different integration areas, changing the position of the virtual knife edge in the software, and confirmed that the results were similar within the statistical errors.

There are also systematic errors due to pixel-to-pixel non-uniformity and focus precision. The pixel-to-pixel uniformity error was found to be small. The focus drifted by small amounts, but not significantly during scans.

We investigated statistical uncertainties due to shot noise and read noise. The read noise was on the order of 20 analog to digital units (ADUs), small compared to the shot noise on the signal, which varied from 2-5% for most substrate voltages. The measurement error was dominated by the statistical uncertainties on the data points due to shot noise; in future work, this could be further reduced by taking more data points.

VI. Conclusions

We have measured the image degradation effects due to lateral charge diffusion in thick, fully-depleted CCDs. The experimental data motivated a modification of the theory to correctly account for velocity saturation effects. We have created a stable experimental setup for measuring charge diffusion in CCDs, which will be useful for many future investigations. Our measurement, at a substrate voltage of 115 V, of a diffusion of 3.71 ± 0.16 μm is very promising for the performance capabilities of these CCDs and meets the SNAP requirements.

Future work will include intrapixel response studies, measurements of effects at the edge pixels of the CCD, and investigation of near infrared lateral charge diffusion.

Acknowledgment

We would like to thank Stephen Bailey, Chris Bebek, Don Groom, Stephen Holland, Armin Karcher, Bill Kolbe, Wolfgang Lorenzon, and Natalie Roe for guidance with the experimental technique and theory.

References

[1] S. Holland et al., "Fully-Depleted, Back-Illuminated Charge-Coupled Devices Fabricated on High-Resistivity Silicon", 2003, IEEE Trans. Electron Dev. 50 (3).

[2] A. Karcher et al., "Measurement of Lateral Charge Diffusion in Thick, Fully Depleted, Back-illuminated CCDs," 2004, IEEE Trans. Nucl. Sci. 51 (5).

[3] G. Aldering et al., "Overview of the Supernova/Acceleration Probe (SNAP)", 2002, SPIE Proceedings. G. Aldering et al., "Overview of the Supernova/Acceleration Probe (SNAP)", 2002, SPIE Proceedings.

[4] D. Groom et al., "Point-spread function in depleted and partially depleted CCDs", 1999, SPIE Proceedings.

[5] C. Jacoboni et al., "A Review of Some Charge Transport Properties of Silicon", 1977, Solid State Electronics Vol.20 pp. 77-89.

Figures

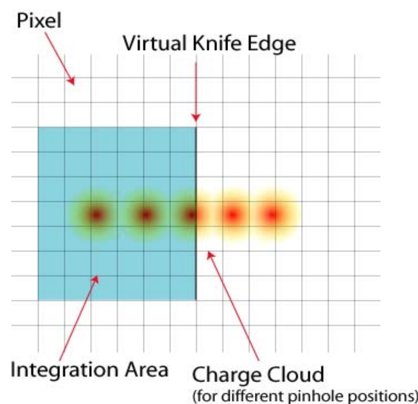

Figure 1. Virtual knife edge principle.

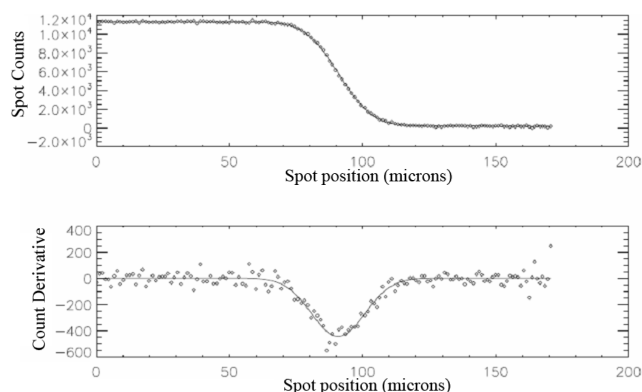

Figure 2. Sample scan analysis. The top plot is the measured CCD counts in the integration region versus the beam position; the bottom plot is the derivative of the top, showing a Gaussian response function which is fit to obtain the rms diffusion.

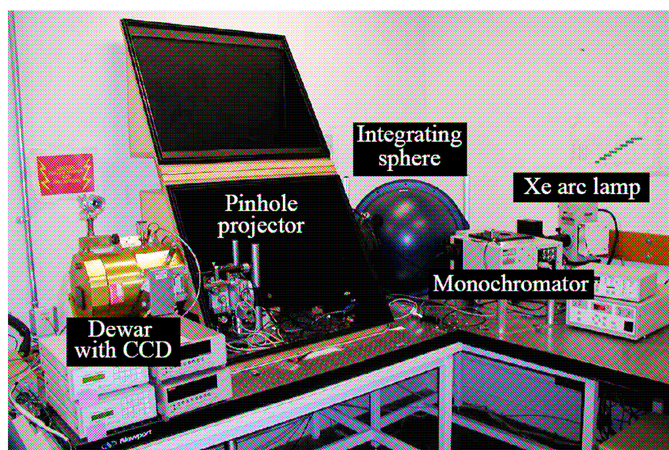

Figure 3. The experimental setup.

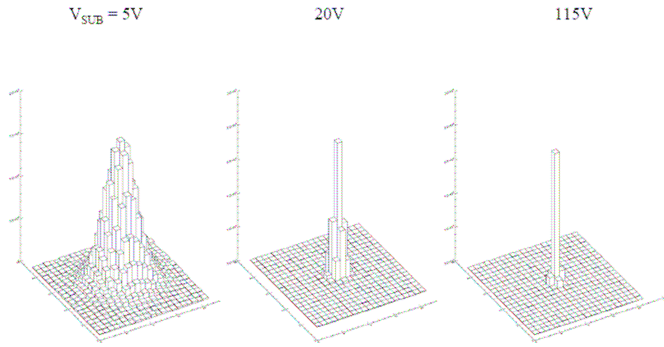

Figure 4. The spot image for three different substrate bias voltages. Full depletion is reached at 20 V.

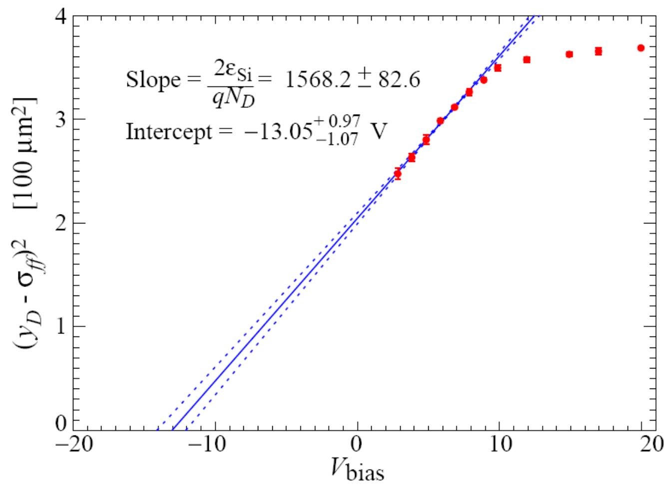

Figure 5. The low-voltage linear fit used to determine parameters for the high-voltage fit. Here the square of the wafer thickness minus diffusion is plotted against the substrate voltage. The x-intercept gives the junction voltage, and the slope gives the carrier density.

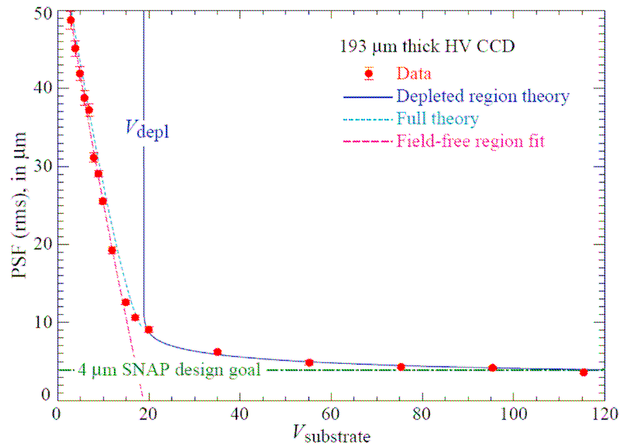

Figure 6. The measured rms diffusion as a function of the substrate bias voltage; the data are the red points, the magenta curve is the theoretical fit for operation below full depletion, the dark blue curve is the theoretical prediction for over-depleted operation, and the light blue curve is the convolution of both curves.

V_{sub} (V)	Diffusion (μm)	Error (μm)
2.84	48.77	1.12
3.82	45.14	0.99
4.83	41.93	0.85
5.83	38.79	0.90
6.84	37.25	0.80
7.87	31.14	0.58
8.89	29.07	0.39
9.86	25.55	0.37
11.91	19.29	0.44
14.90	12.62	0.28
16.96	10.67	0.29
19.94	9.12	0.34
35.04	6.29	0.26
55.20	4.93	0.29
75.30	4.39	0.17
95.40	4.29	0.17
115.40	3.71	0.16

Table 1. The measured rms diffusion, with beam size subtracted in quadrature, and experimental errors plotted in Figure 5.